Available online at www.sciencedirect.com
ScienceDirect
Journal of Photochemistry and Photobiology A: Chemistry 194 (2008) 161–166
Journal of Photochemistry and Photobiology A:Chemistry
www.elsevier.com/locate/jphotochem

Modified electrode architecture for efficient and air-stable polymer solar cells based on P3HT:PCBM

Seok-In Na, Seok-Soon Kim, Jang Jo, Ki-Sung Lee, Seong-Ju Park, Dong-Yu Kim *

Heeger Center for Advanced Materials, Department of Materials Science and Engineering, Gwangju Institute of Science and Technology, 1 Oryong-Dong, Buk-Gu, Gwangju 500-712, South Korea

Received 20 April 2007; received in revised form 26 June 2007; accepted 1 August 2007
Available online 6 August 2007

Abstract

Data are presented on high performance and air-stable organic solar cells with modified electrode architecture (MAOSCs), which have a patterned transparent anode determining the real active area of devices and a large area of reflective cathode covering the whole area of an active layer based on poly(3-hexylthiophene) (P3HT) and 1-(3-methoxycarbonyl)-propyl-1-phenyl-(6,6)C61 (PCBM). Based on the finite-difference time-domain (FDTD) scheme as a numerical method, improved light trapping within the photoactive layer, resulting from the efficient reflection of incident light at the large area of cathode, can be attained by modifying the conventional organic solar cell structures. Here, an improved power conversion efficiency of 4.3% was obtained in the case of MAOSCs under 1 Sun with air mass (AM) 1.5 global (G) condition. In addition, the stability of MAOSCs in air was remarkably improved due to the limited exposure of their active layers to air.

Keywords: Organic solar cells; Bulk heterojunction; Modified architecture; Light trapping; Stability

1. Introduction

Since their introduction [1–3], organic solar cells (OSCs) based on small molecules and conjugated polymers have undergone considerable development, including improvements in organic synthesis and fabrication technologies, thus providing a chance to enhance the power conversion efficiency. Among the class of conjugated polymer-based solar cells [4–8], one of the most attractive systems under recent consideration is the P3HT and PCBM bulk heterojunction [5–8]. As is well-known, 4–5% power conversion efficiencies of OSCs under 80 or 100 mW/cm^2 illuminations with AM 1.5 G conditions have been reported in recent years. However, several problems such as a severe mismatch between the spectrum of the polymer and solar spectrum, poor stability, phase segregation, and low mobility of charge carriers must be still overcome [9–11].

Typically, P3HT and PCBM based heterojunction OSCs are fabricated by solution processes, including spin-coating, dip-coating, and doctor blading, with an active film thickness of about a few tens of nanometers to ~200 nm. It is widely believed that this active layer should be thick enough (~240 nm) to absorb most of the solar radiation over the wavelengths of 450–600 nm [11]. However, a thick active layer results in the increase of series resistance of the device due to the limited charge carrier mobility of conjugated polymers. This indicates that a trade-off exists between the absorption of incident light and series resistance, leading to a compromised OSC design that limits the power conversion efficiency (η_p) of OSCs. Hence, approaches for novel device design to achieve light trapping within active layer to maximize the use of incident light illuminated into the solar cell have been suggested [12–15]. Until now, there are only a few approaches for light trapping in case of OSCs, in contrast to the Si solar cell. For example, Roman et al. showed that soft embossed gratings result in enhanced light trapping in photodiodes [12] and more recently, Cocoyer et al. reported that the introduction of submicrometric periodic surface structures leads to the enhancement of the absorption of organic photovoltaic cells [13]. However, one of the most preferential and the simplest implementations of light trapping concept is to optimize the backside metallization for high reflectance, ensuring that the incident light will cross the cell twice [14].

Here, we demonstrate organic solar cells with modified electrode architecture (MAOSCs) with improved efficiency and enhanced air-stability. As compared to the conventional OSCs,

* Corresponding author. Tel.: +82 62 970 2319; fax: +82 62 970 2304.
E-mail address: kimdy@gist.ac.kr (D.-Y. Kim).

1010-6030/$ – see front matter © 2007 Elsevier B.V. All rights reserved.
doi:10.1016/j.jphotochem.2007.08.003

having a whole area of transparent conducting oxide (TCO) anode and a patterned small area of reflective metal cathode determining the real active area of devices, MAOSCs reported here are fabricated with a patterned TCO determining the real active area of devices and a whole area of reflective metal cathode which is evaporated onto the active layer. In the MAOSC design, the entire incident light is redirected to the active layer through efficient reflection from a whole area of metal cathode covering the entire active layer, leading to improved efficiency as a result of enhanced light absorption. Furthermore, due to the encapsulation effect provided by covering a whole area of the active polymer layer with the metal cathode, air exposure of the oxidatively weak conjugated polymer is efficiently reduced; consequently enhanced stability can be expected.

2. Experimental

From Fig. 1, it can be seen that the proposed MAOSCs consist of five layers; the same structure as conventional OSCs except for the inverted area of two electrodes. After successive cleaning in an ultrasonic bath with acetone and isopropyl alcohol for 20 min, followed by drying in nitrogen stream, photolithography and wet-etching processes were performed on the indium-tin-oxide (ITO-Samsung Corning Co., Ltd.) coated glass for the preparation of the patterned TCO anode to produce an active area of 0.0434 cm^2, by using a Cr mask and $HCl/HNO_3/H_2O$ mixture as a wet-etching solution. Then, the ITO coated glass substrates were cleaned again by a special detergent, followed by ultrasonification with an organic solvent. Before commencing OSC fabrication, the cleaned substrates were baked in a convection oven at 110 °C for about 12 h.

Bulk heterojunction solar cells with and without modified architecture were fabricated according to the following procedures. First, ITO was treated with O_2 plasma for the formation of a hydrophilic surface. Next, poly(3,4-ethylenedioxythiophene):poly(styrenesulfonate) (PEDOT:PSS, Baytron P VPAI 4083) was spin-coated onto ITO with a thickness of ~20 nm from an aqueous solution after passing through a 0.45 μm filter, followed by drying at 120 °C for 10 min in air. The PEDOT:PSS layer was used only to improve hole-transport and reduce the probability for electrical shorts. A chlorobenzene solution comprised of P3HT and PCBM with a 1:0.5 weight ratio was then spin-coated on top of the PEDOT:PSS layer, and annealed at 110 °C for 10 min to enhance the degree of ordering of P3HT [7]. The P3HT and the PCBM were purchased from Rieke Metals and Nano-C, respectively. The molecular weight and polydispersity index of P3HT are ~40000 and ~1.5, respectively. Finally, the reflective metal cathode consisting of 100 nm Ag on top of 20 nm Ca was thermally evaporated through a shadow mask to produce an active area of 0.0434 cm^2 and without the shadow mask for the fabrication of conventional OSCs and MAOSCs, respectively, in a vacuum at 10^{-6} Torr. Here, we have carefully controlled the processes to produce the same real active area (0.0434 cm^2) for both conventional OSCs and MAOSCs, as shown in Fig. 1.

Cell performance was measured under 1 Sun using a xenon light source and an AM 1.5 global filter. Photocurrent–voltage (*I–V*) measurements were performed using a Keithley 4200 instrument in air. A calibrated silicon reference solar cell certificated by the National Renewable Energy Laboratory (NREL) was used to confirm the measurement conditions of our set-up.

The optical properties of photoactive layers spin-coated onto the whole area of ITO and patterned ITO were investigated via UV/vis absorption spectral measurements at room temperature with a Perkin-Elmer Lambda 12 UV/vis spectrophotometer. For modeling of light propagation in OSC and MAOSC, the FDTD

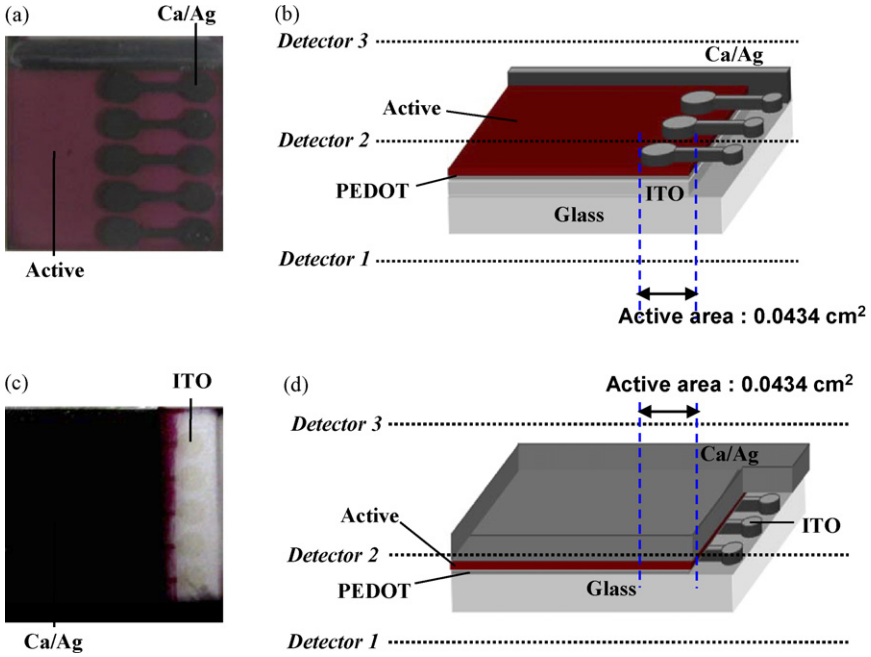

Fig. 1. A plan-view photomicrograph and schematic cross-sectional representation of the conventional organic solar cells (OSCs) (a and b) and organic solar cells with modified architecture (MAOSCs) (c and d).

method was applied [16–19]. In addition, the stability of OSCs and MAOSCs was compared in air for 2520 min without any encapsulation of either cell.

3. Results and discussion

First, based on the finite-difference time-domain (FDTD) scheme as a numerical method, light profile within the photoactive layer was investigated [16–19]. The FDTD method solves Maxwell's equations by first discretizing the equations via central differences in time and space, and then numerically solving these equations by use of software. In order to use the FDTD algorithm to study the propagation of the light in each conventional OSC and MAOSC structure shown in Fig. 1, the physical, material, and numerical parameters such as the thickness and refractive index of the layers involved are all considered. Moreover, the plan wave as normal incident light starting from glass is applied, with a wavelength of 500 nm. Fig. 2 presents the light propagation. Each photon detector (Detector 1, 2 and 3) is located under glass, in the middle of the active layer, and on top of the reflective cathode, respectively, as shown in Fig. 1. The monitor value refers to the quantity of the total photons calculated by each detector and cT (μm) means that the unit of time changes as a unit of distance, where c is the speed of the light in a vacuum ($\sim 3 \times 10^{14}$ μm/s).

As expected, the monitor value of Detector 1 in MAOSC increases when compared to that of the conventional OSC, as shown in Fig. 2(a and b), because almost all photons are redirected down due to the large area of the reflective cathode covering the whole active layer. Moreover, MAOSC Detector 3 indicates that few photons exist on top of the reflective cathode, whereas Detector 3 of the conventional OSC shows a similar profile for the propagating light as Detector 2 as most of the detected photons in the middle of the active layer go out through the active layer, as shown in Fig. 2(a). But, interestingly, the light profile in the middle of the active layer (Detector 2) of MAOSC was seen to continuously change, with an oscillatory nature, as shown in Fig. 2(b). This variance indicates that photons can move around the active area for a long time. Consequently, the increased probability and ability to trap the light in the active area was confirmed by simulation based on FDTD and an improvement of photocurrent and efficiency of devices could be expected [20–22].

Fig. 3 presents the resulting current–voltage characteristics of conventional OSCs and MAOSCs. Here, two kinds of active layer having thicknesses of ~90 and ~160 nm were prepared by controlling the spin rate in order to observe the effect of active layer thickness on the performance of the conventional OSCs and MAOSCs. Detailed information on the open circuit voltage (V_{oc}), photocurrent density (J_{sc}), fill factor (FF) and η_p is listed in Table 1. In the case of conventional OSCs, even though the photocurrent was increased by increasing the active layer thickness from ~90 to ~160 nm, the η_p was not improved. This can be attributed to a decrease in the FF value from 57.0 to 50.4% due to an increase in the total series resistance resulting from a corresponding increase in the active thickness. As is well-known, because the FF is limited by the carrier drift length, a high mobil-

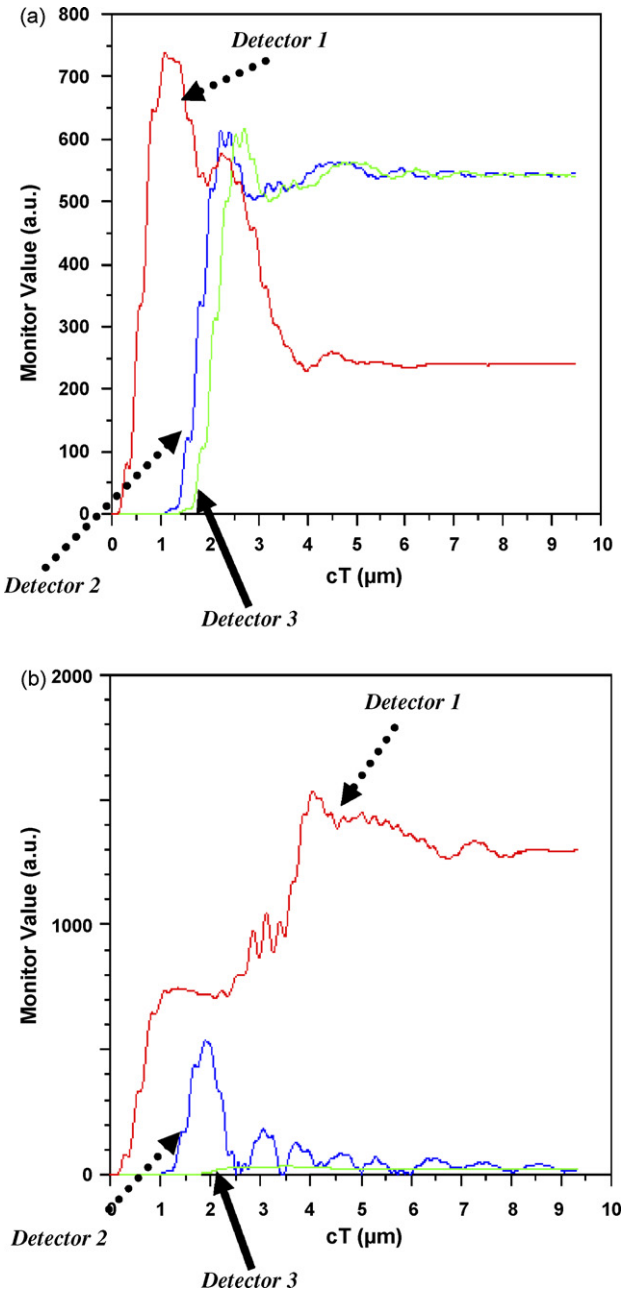

Fig. 2. The light profile simulated by computational steps of FDTD in (a) the conventional OSC structure and (b) the MAOSC structure. Each detector was located under the glass (Detector 1), in the middle of the active layer (Detector 2), and on the top of the reflective cathode (Detector 3), respectively, as shown in Fig. 1(b and d).

Table 1
Photovoltaic parameters and efficiencies of conventional OSCs and MAOSCs with two different thicknesses of the active layer (P3HT:PCBM)

	Thickness (nm)	V_{oc} (V)	J_{sc} (mA/cm^2)	FF (%)	η_p (%)
Conventional OSC	~160	0.638	10.1	50.4	3.25
	~90	0.642	9.10	57.0	3.33
MAOSC	~160	0.630	12.01	49.2	3.72
	~90	0.634	12.3	55.1	4.30

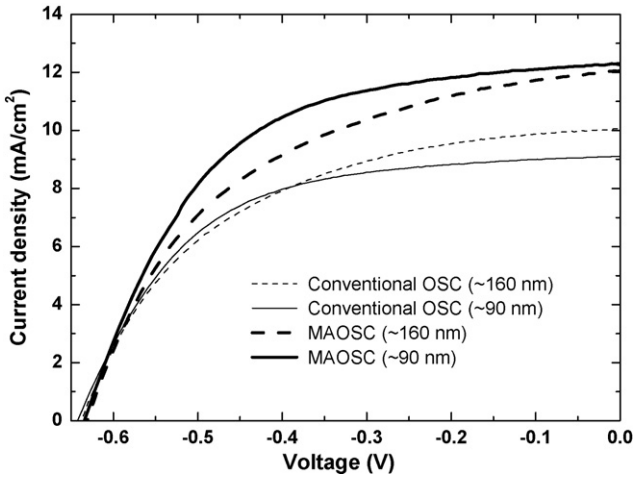

Fig. 3. Current–voltage characteristics of conventional OSCs and MAOSCs in air under the standard illumination condition (100 mW/cm^2 with AM 1.5 G conditions).

ity of carriers or thin film is necessary for efficient charge carrier extraction without the significant loss from recombination [9].

In the case of MAOSCs, the J_{sc} values of two kinds of MAOSCs, with ~90 and ~160 nm thick active layers, were comparable and these J_{sc} values increased as compared to both thin and thick conventional OSCs. On the other hand, the FF of MAOSCs was slightly lower compared to the conventional OSC with the same thickness. It is attributed to the increased resistance, resulting from the reduced area of the ITO by patterning. Specially, the η_p of the MAOSC with ~90 nm thin active layer was dramatically increased (4.30%), as compared to that of the conventional cell (3.33%), as a result of the increased photocurrent density. The η_p of the MAOSC was enhanced about 1.3 times when compared to that of the conventional OSC, even without optimization of electrodes [23]. The η_p of the conventional OSC with a Ca/Ag cathode electrode is similar to that of the previous report [24]. The efficiency variation of the conventional OSCs and MAOSCs is all within ±0.2% under 100 mW/cm^2.

The increased J_{sc} value of MAOSCs indicates the increased charge generation, resulting from the enhanced ability of active materials to absorb the incident light via light trapping, as observed in the FDTD simulation result. In other words, because of the large area of the reflective cathode covering the whole area of the active layer, incident light is redirected to the active layer from the cathode; consequently the photon could be trapped more effectively in the active layer, ultimately resulting in increased light absorption of active materials. In addition, because of the reduced ITO anode area, loss of incident light, caused by reflection at the interface and absorption by ITO, can be decreased and this reduced loss of incident light can also affect the photocurrent of devices.

To investigate the effect of the reduced area of ITO on the photocurrent, the absorbance of conventional OSCs and MAOSCs was measured by the UV/vis absorption spectra. Fig. 4(a) shows the UV–vis absorption spectra of P3HT:PCBM on the unpatterned and patterned ITO coated glass substrates and Fig. 4(b) exhibits the absorption spectra of the substrates. The lower

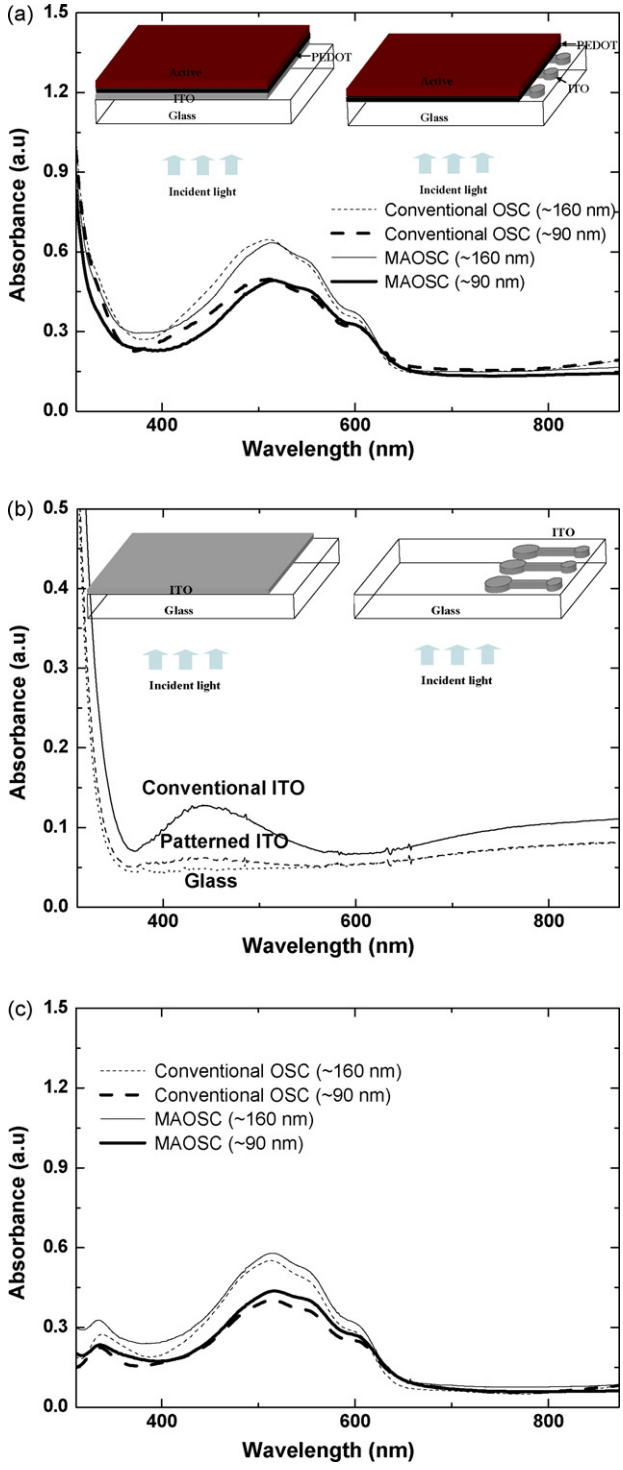

Fig. 4. (a) UV–vis absorption spectra of active materials coated onto the conventional and patterned ITO coated glass substrates. (b) UV–vis absorption spectra of the conventional and patterned ITO coated glass substrates. (c) The absorption spectra of active materials extracted by subtracting the absorption by ITO coated glass substrates (Fig. 3(b)) from the absorption spectra of active materials on the ITO coated glass substrates (Fig. 3(a)).

absorption of P3HT in the range of ~400–500 nm was observed in the absorption spectra of the active layer on the patterned ITO substrate. The lower absorption in this wavelength region is attributed to the decreased absorption of ITO resulted from

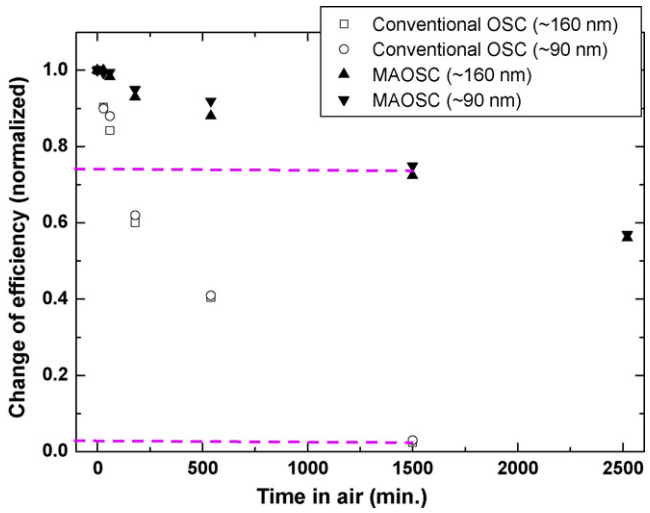

Fig. 5. The efficiencies of two types of conventional OSCs and MAOSCs measured in air for 2520 min.

the reduced area of ITO by patterning, as shown in Fig. 4(b). To compare the effective light absorption by P3HT in both devices, Fig. 4(c) was extracted by subtracting the absorption by ITO coated glass substrates (Fig. 4(b)) from the absorption spectra of active materials on the ITO coated glass substrates (Fig. 4(a)). Fig. 4(c) shows the slightly enhanced absorption spectrum of P3HT in MAOSCs resulted from the smaller ITO area of MAOSCs than that of conventional OSCs. Therefore, more efficient light absorption was possible by reducing the ITO area. However, considering the dramatically increased J_{sc} of the MAOSC, the effect of enhancement in absorption by changing the ITO architecture can be considered very small.

Furthermore, in the case of MAOSCs, by applying the large area metal electrode covering a whole area of the active polymer layer, the encapsulation effect limiting the exposure of the active layer to air can be expected. The change of efficiencies with an increase in time (minutes) for two types of conventional OSCs and MAOSCs was investigated, as shown in Fig. 5. During the measurement of stability, the samples were kept in air without any encapsulation, with humidity kept between 45 and 55%. As shown in the figure, the efficiencies of conventional OSCs dramatically decreased compared to those of MAOSCs due to the degradation under air exposure, mostly resulting from the water adsorption [25]. Specifically, after air exposure for 1500 min, conventional OSCs have ~0% of their original values, similar to those of the recent report [25], whereas two MAOSCs still show a relatively good efficiency of over 70% of their original values. This ability to maintain efficiency indicates that the stability of the active layer is dramatically improved due to the large area reflective cathode (Ca/Ag) covering the entire active layer in the MAOSC, decreasing the chance of exposure to detrimental conditions such as oxygen and moisture. Considering the current state of technology based on the OSCs with efficiencies approaching ~5%, a commercialization of OSCs could be come true in the near future. One of the crucial points needed for practical device applications of OSCs is the stability in the ambient conditions. Studies on the stability of OSCs have typically focused on the optimization of the encapsulated devices, and the encapsulation process is usually performed in the glove box to limit the degradation of the efficiency by exposure to air [25,26]. Based on this situation, our modified architecture of OSCs showing both improved efficiency and excellent stability in air can be considered as a promising structure for the commercially applicable OSCs with an easier and more effective encapsulation process in air.

4. Conclusions

In summary, high performance MAOSCs, having a large area reflective metal cathode covering the entire active layer based on the P3HT and PCBM bulk heterojunction, have been demonstrated. Based on the simulations in FDTD, improved photon trapping within photoactive layers can be expected in MAOSCs. In addition, newly designed OSCs also exhibit improved air-stability due to the limited exposure of the active layer. To this extent, an improvement in η_p of 4.3% was obtained in the case of MAOSCs, and an efficiency of over ~70% of the original values was maintained after exposure in air for 1500 min.

Acknowledgements

This work was supported by Heeger Center for Advanced Materials (HCAM), the Ministry of Education of Korea through Brain Korea 21 (BK21) program, the Korea Science and Engineering Foundation (KOSEF) through the National Research Lab. Program funded by the Korea government (MOST) (M10500000077-06J0000-07710), and MOCIE (Ministry of Commerce, Industry and Energy of the Korean Government) (10022811).

References

[1] C.W. Tang, Appl. Phys. Lett. 48 (1986) 183.
[2] N.S. Sariciftci, L. Smilowitz, A.J. Heeger, F. Wedl, Science 258 (1992) 1474.
[3] G. Yu, J. Gao, J.C. Hemmelen, F. Wudl, A.J. Heeger, Science 270 (1995) 1789.
[4] C.J. Brabec, N.S. Sariciftci, J.C. Hummelen, Adv. Funct. Mater. 11 (2001) 15.
[5] T. Yamanari, T. Taima, K. Hara, K. Saito, J. Photochem. Photobiol. A-Chem. 182 (2006) 269.
[6] X. Yang, J. Loos, S.C. Veenstra, W.J.H. Verhees, M.M. Wienk, J.M. Kroon, M.A.J. Michels, R.A.J. Janssen, Nano Lett. 5 (2005) 579.
[7] Y. Kim, S.A. Choulis, J. Nelson, D.D.C. Bradley, S. Cook, J.R. Durrant, Appl. Phys. Lett. 86 (2005) 063502.
[8] F. Padinger, R.S. Rittberger, N.S. Sariciftci, Adv. Funct. Mater. 13 (2003) 85.
[9] W. Ma, C. Yang, X. Gong, K. Lee, A.J. Heeger, Adv. Funct. Mater. 15 (2005) 1617.
[10] M. Reyes-Reyes, K. Kim, J. Dewald, R. López-Sandoval, A. Avadhanula, S. Curran, D.L. Carroll, Org. Lett. 7 (2005) 5749.
[11] G. Li, V. Shrotriya, J. Huang, Y. Yao, T. Moriarty, K. Emery, Y. Yang, Nat. Mater. 4 (2005) 864.
[12] L.S. Roman, O. Inganäs, T. Granlund, T. Nyberg, M. Svensson, M.R. Andersson, J.C. Hummelen, Adv. Mater. 12 (2000) 189.
[13] C. Cocoyer, L. Rocha, L. Sicot, B. Geffroy, R. de Bettignies, C. Sentein, C. Fiorini-Debuisschert, P. Raimond, Appl. Phys. Lett. 88 (2006) 133108.

[14] L.D. Partain (Ed.), Solar Cells and Their Applications, John Willy & Sons, 1995.
[15] S.S. Sun, N.S. Sariciftci (Eds.), Organic Photovoltaics: Mechanism, Materials, and Devices, Taylor & Francis, 2005.
[16] K.S. Yee, IEEE Trans. Antennas Propagat. 14 (1966) 302.
[17] J.P. Berenger, J. Compt. Phys. 114 (1994) 185.
[18] B. Lehner, K. Hingerl, Thin Solid Films 455–456 (2004) 462.
[19] P.R. Villeneuve, S. Fan, J.D. Joannopoulos, Phys. Rev. B 54 (1996) 7837.
[20] F. Llopis, I. Tobías, Sol. Energy Mater. Sol. Cells 87 (2005) 481.
[21] T. Marshall, M. Piket-May, Appl. Comput. Electrochem. Soc. J. 12 (1997) 31.
[22] C. Beneking, B. Rech, S. Wieder, O. Kluth, H. Wagner, W. Frammelsberger, R. Geyer, P. Lechner, H. Rűbel, H. Schade, Thin Solid Films 351 (1999) 241.
[23] C.J. Brabec, S.E. Shaheen, C. Winder, N.S. Sariciftci, P. Denk, Appl. Phys. Lett. 80 (2002) 1288.
[24] R. de Bettingnies, J. Leroy, M. Firon, C. Sentein, Proc. SPIE 5938 (2005) 59380C.
[25] K. Kawano, R. Pacios, D. Poplavskyy, J. Nelson, D.D.C. Bradely, J.R. Durrant, Sol. Energy Mater. Sol. Cells 90 (2006) 3520.
[26] F.C. Krebs, Sol. Energy Mater. Sol. Cells 90 (2006) 3633.